CHINESE JOURNAL OF PHYSICS

ISSN: 0577-9073

Impact factor = 1.051

Publisher = Elsevier

ACCEPTED FEBRUARY 11TH 2019

EFFECTS OF COAGULATION ON THE TWO-PHASE PERISTALTIC PUMPING OF MAGNETIZED PRANDTL BIOFLUID THROUGH AN ENDOSCOPIC ANNULAR GEOMETRY CONTAINING A POROUS MEDIUM

M. M. Bhatti[1,2*], A. Zeeshan[3], R. Ellahi[3,4], O. Anwar Bég[5] and A. Kadir[5]

[1]*Shanghai Institute of Applied Mathematics and Mechanics, Shanghai University, Shanghai 200072, China*

[2]*Shanghai Key Laboratory of Mechanics in Energy Engineering, Yanchang Road, Shanghai 200072, China*

[3]*Department of Mathematics, International Islamic University, Islamabad, Pakistan*

[4]*Center for Modeling & Computer Simulation, Research Institute, King Fahd University of Petroleum & Minerals, Dhahran-31261, Saudi Arabia.*

[5]*Department of Aeronautical and Mechanical Engineering, School of Computing, Science and Engineering, Salford University, Manchester, M54WT, UK.*

**Corresponding author: Email: muhammad09@shu.edu.cn; mubashirme@yahoo.com*

Abstract: In this article, motivated by more accurate simulation of electromagnetic blood flow in annular vessel geometries in intravascular thrombosis, a mathematical model is developed for elucidating the effects of coagulation (i.e. a blood clot) on *peristaltically induced motion of an electrically-conducting (magnetized) Prandtl fluid physiological suspension through a non-uniform annulus containing a homogenous porous medium*. Magnetohydrodynamics is included owing to the presence of iron in the hemoglobin molecule and also the presence of ions in real blood. Hall current which generates a secondary (cross) flow at stronger magnetic field is also considered in the present study. A small annular tube (endoscopic) with sinusoidal peristaltic waves traveling along the inner and outer walls at constant velocity with a clot present is analyzed. The governing conservation equations which comprise the continuity and momentum equations for the fluid phase and particle phase are simplified under lubrication approximations (long wavelength and creeping flow conditions). The moving boundary value problem is normalized and solved analytically (with appropriate wall conditions) for the fluid phase and particle phase using the homotopy perturbation method (HPM) with **MATHEMATICA** software. Validation is conducted with **MAPLE** numerical quadrature. A parametric study of the influence of clot height

(δ), particle volume fraction (C), Prandtl fluid material parameters (α, β), Hartmann number (M), Hall parameter (m), permeability parameter (k), peristaltic wave amplitude (φ) and wave number ($\bar{\delta}$) on pressure difference and wall shear (friction forces) is included. Pressure rise is elevated with clot height, medium permeability and Prandtl rheological material parameters whereas it is reduced with increasing particle volume fraction and magnetic Hartmann number. Friction forces on the outer and inner tubes of the endoscope annulus are enhanced with clot height and particle volume fraction whereas they are decreased with Prandtl rheological material parameters, Hall parameter and permeability parameter. The simulations provide a good benchmark for more general computational fluid dynamics studies of magnetic endoscopic multi-phase peristaltic pumping.

Keywords: *Magnetic endoscopy; Prandtl rheological model; Particle-fluid suspension; Peristaltic waves; Magneto-hemodynamics; particle volume fraction; Hall current; permeable medium; pressure difference; wave amplitude; friction force; homotopy perturbation method (HPM), Maple quadrature.*

1. INTRODUCTION

Hemodynamics has emerged as a vibrant sub-field in modern fluid mechanics. It involves the theoretical, computational and experimental (clinical) analysis of how blood flows in the cardiovascular and capillary systems. An important aspect of healthy blood flow is the circumvention of a thrombus i.e. blood clot which is the ultimate product of blood coagulation in hemostasis [1-2]. In this scenario, blood platelets quickly conglomerate at the location of a vascular injury. The vessel wall and sub-endothelium rapidly attach to the developing thrombus. Subsequent to clot retraction, damaged tissue decreases the clot permeability and curtails blood leakage. Clots may also arise in hemodynamic devices and medical blood processing systems. The hemodynamics associated with clot contraction and subsequent modification in blood flow dynamics is complex and involves many different fluid mechanical aspects including multi-phase characteristics, laminar and turbulent flow, separation, vortex dynamics etc. [3-4]. Magnetically Guided Capsule Endoscopy (MGCE) has also emerged as a promising new development in biomedical engineering in which is body-exogenous magnetic fields are exploited to manipulate transport in various digestive tract and other physiological system diagnoses. The presence of, for

example, ions in digestive fluids and iron in the hemoglobin molecule make these physiological fluids responsive to the application of external magnetic fields. The resulting flows are *magnetohydrodynamic* in nature and as such are amenable to the application of advanced diagnostic and therapeutic functionalities in monitoring the function of these biological systems [5,6]. In improving the performance of magnetic biomedical technology, *magneto-fluid dynamic simulation* plays a critical role since it is non-invasive and multiple scenarios can be studied relatively inexpensively. Most endoscopic designs comprise an *annular geometry* with deformable walls. The walls distend to generate peristaltic motion which allows navigation of the device intelligently. The technology has been widely embraced worldwide and includes the Siemens-Olympus design (Siemens Medical, Erlangen, Germany and Olympus America, Center Valley, Pennsylvania, USA) [7] which consists of a guidance magnet, an image processing and guidance information system (console viewed by the operator and a scanner for the patient to lie in), and a capsule endoscope. The magnet system generates varying magnetic fields which can be very precisely regulated via a smart "joystick" to navigate the capsule. Cameras at both ends of the capsule transmit images. This constitutes an excellent real-world clinical example of *annular magnetohydrodynamic peristaltic propulsion*. Electromagnetic pumping flows of this type also feature in numerous other magneto-biomedical engineering devices including extra-corporeal surgical control, bio-magnetic therapy, nano-pharmacological delivery systems etc [8-10].

To optimize such magnetohydrodynamic medical devices, it is important to continuously develop *robust mathematical multi-physical magnetohydrodynamic peristaltic pumping models*. Furthermore, the working fluids in the annular space may be *heated, contain suspensions and manifest a variety of electromagnetic effects depending on the strength of the administered magnetic field e.g. Hall currents, Maxwell displacement currents etc*. All these aspects must be correctly simulated to provide a complete picture of the hydrodynamic processes intrinsic to efficient pumping performance. In the formulation of such models either nonlinear partial or ordinary differential equation boundary value problems arise. These require advanced analytical or numerical methods for their robust solution. A comprehensive review of such methods for a wide spectrum of magnetofluid dynamics problems including medical, energy, aerospace and materials processing has been presented by D'Ambrosio and Giordano [11].

Central to the successful operation of the magnetic endoscope biomedical device is *peristalsis*. Peristalsis [12] is a mechanism utilized for both internal transport of biological liquids and also

external animal motion, that arises when smooth muscles in a living body or artificially engineered device contract and expand along the length of a conduit e.g. channel, tube. It is a hereditary property in various biological systems which feature smooth muscles that permit the trans-location of many kinds of biological fluids (e.g. blood, semen, chyme) by a rhythmic propulsive action. This mechanism also characterizes urine transport in the excretory system (kidney to bladder), vasomotion of tiny blood vessels in the capillary system, cardio-vascular pumping in the embryonic heart etc. Additionally, it features in the movement in phloem in trees and plants and the locomotion of earthworms and snakes. Owing to the exceptional efficiency of the peristaltic process, it has been frequently mimicked in various industrial applications. Examples include blood pumps, hazardous waste (sanitary, corrosive, nuclear fluid) pumps, rocket fuel connection systems (for preventing backflow of fuels) etc. Important experimental studies concerning peristalsis have been communicated, notably by Shapiro *et al.* [13] and Brown and Hung [14] Various authors have analyzed the peristaltic motion of various biological fluids in different geometrical configurations. For instance, Vajravelu *et al*. [15] investigated the peristaltic motion of second order fluid through a tube. Vajravelu *et al.* [16] examined the peristaltic flow with heat transfer through a vertical porous annulus. Akbar and Nadeem [17] explored the peristaltic transport of Phan-Thien-Tanner (PTT) nanofluid through a diverging tube. Tripathi *et al.* [18] studied the peristaltic channel flow of a viscoelastic fluid with a fractional Maxwell model. Series solutions for magnetic peristaltic flow of non-Newtonian Jeffrey fluid through an eccentric cylinder were derived by Ellahi *et al.* [19]. Other investigations of annular magnetohydrodynamic peristaltic pumping flows in non-Newtonian media have been communicated in [20]-[25] with multi-physics included (heat transfer, mass transfer, rheology etc).

The multi-phase nature of real blood makes it extremely sophisticated and difficult to simulate precisely with fluid dynamic models. Blood is often approximated as a *particle-fluid suspension* (platelets immersed in plasma) and the platelets exhibit deformation during motion and also from interaction with surfaces. For example, red blood cell behavior at the mesoscopic scale plays a critical role in different pathological and physiological mechanisms in the microcirculation. These include thrombo-genesis in which the rotation and transverse motion of red blood cells in shear is critical. According to theoretical and experimental studies [26, 27], blood in narrow arteries cannot be treated as a homogeneous Newtonian single-phase fluid. It is therefore necessary to simulate blood flow in narrow conduits as a non-Newtonian two-phase fluid (particle-fluid suspension).

The annular channel designs in magnetic endoscopes are also very narrow and similar methodologies should be applied in simulating hemodynamic pumping. Accurate constitutive modelling is therefore recommended for improving the performance of such devices and leads to significant benefits in clinical engineering [28]. Two-phase hemodynamic transport has been extensively studied by engineering scientists with many different analytical and computational methods in recent decades. Examples include peristaltic flows [29], geometric design of bypass graft-ends and the prediction of local aerosol depositions in the human upper airways [30], coronary atherogenesis arterial dynamics [31], annular peristaltic flows [32], magnetohydrodynamic Hall current pulsatile-peristaltic hemodynamics [33], dialysis filtration simulation [34], slip endoscopic peristaltic pumping flows [34], thermal purification biomedical systems modelling [35]. Further examples include blood purification auto-transfusion porous media hybrid devices [36], electro-conductive geothermal buoyancy-driven flows [37], eccentric peristaltic annular pumping [38], variable-viscosity clot peristaltic hemodynamics [39] and viscoelastic slip magneto-hemodynamic peristaltic pumping in straight and curved ducts [40, 41].

As elaborated earlier, endoscopy is also a very important diagnostic device in medical engineering and has also stimulated some attention in mathematical modelling. In terms of fluid dynamics, there is no difference between catheters and endoscopes. Xiong *et al.* [42] employed ANSYS FLUENT computational fluid dynamic (CFD) software to simulate the nasal cavity airflow pre and post-virtual functional endoscopic surgery (FESS). Al Misiery *et al.* [43] deployed perturbation methods to analyze the wave amplitude effects in peristaltic endoscopic flow with the Reynolds exponential viscosity model. Tripathi [44] employed the homotopy perturbation method and variational iteration method to derive solutions for axial velocity, volume flow rate, pressure gradient and stream function in peristaltic endoscopic pumping of generalized Burgers fluids. Hayat *et al*. [45] considered the magnetic peristaltic motion of power-law fluid in an endoscopic geometry. Mekheimer *et al.* [46] studied particle-fluid suspension propulsion by peristaltic waves in an eccentric cylindrical annular endoscope. Rashidi *et al.* [47] utilized the multi-step differential transform algorithm to compute the wave amplitude, Hartmann number and viscoelastic effects in peristaltic transport of electro-conductive viscoelastic fluids in a porous vertical pipe. Tripathi and Bég [48] derived homotopy perturbation solutions for magnetic pumping of Stokes' micro-structural couple stress fluids in endoscopic geometries filled with non-deformable high-

permeability media, observing that pressure is reduced with Stokes coupling and permeability parameters whereas it is enhanced with magnetic Hartmann number and channel width ratio. Further studies include Tripathi *et al.* [49] (on electro-magneto peristaltic pumping of Stokes couple stress fluids in endoscopic tubes) and Rashidi *et al.* [50] (on heat and mass transfer in magnetized blood flow using Casson fluid model).

Inspection of the literature reveals that very few studies have addressed *Hall magnetohydrodynamic fluid-particle suspension pumping by peristaltic waves in an endoscope with clot effects*. Furthermore, the Prandtl non-Newtonian model has thus far not been explored to any great extent in peristaltic rheological simulations. In the present work, therefore, we study the effects of *coagulation (blood clotting) on peristaltic-induced Hall current magnetohydrodynamic transport of a two-phase Prandtl non-Newtonian suspension through a homogenous high-permeability porous medium in the annular geometry of a magnetic endoscope*. The governing flow problem for both fluid and particle phases is mapped from the moving frame to the stationary frame, simplified via lubrication theory, normalized via appropriate transformations and solved as a transformed ordinary differential boundary value problem with the homotopy perturbation method (HPM). Validation with Maple numerical quadrature is included. It is envisaged that the present computations will provide deeper insight into actual magnetic endoscopy hemodynamics and furthermore will furnish a robust benchmark for more general computational fluid dynamics simulations.

2. Magnetic Two-Phase Endoscopic Porous Media Pumping Model

The working biofluid (blood) in the magnetic endoscope annular geometry is considered as the non-Newtonian Prandtl model which contains tiny spherical particles with irrotational, constant and incompressible properties. The biofluid is moving through the inner gap between two co-axial tubes (annular geometry) and these are permeable i.e. wall mass flux is permitted. We adopt a cylindrical coordinate system $(\tilde{r}, \tilde{z})$ in which $\tilde{r}$ designates the radial direction and $\tilde{z}$ the axial coordinate which is orientated along the longitudinal axis of the endoscope, as depicted in **Fig. 1**. The geometry of a wall surface is simulated analytically by the following expressions which realistically describe endoscopic configurations [32, 33, 41, 45]:

$$\left.\begin{aligned}\tilde{r}_1 &= \bar{a}(\tilde{z}) = \begin{cases} a + f\left(\tilde{z},t\right), 0 \le \tilde{z} \le \lambda, \\ a, \text{otherwise} \end{cases}, \\ \tilde{r}_2 &= \tilde{a}\sin 2\pi\lambda^{-1}\left[-ct+\tilde{z}\right]+b(\tilde{z}), \end{aligned}\right\} \tag{1}$$

and

$$b(\tilde{z}) = b_0 + \mathbf{K}\tilde{z}, \tag{2}$$

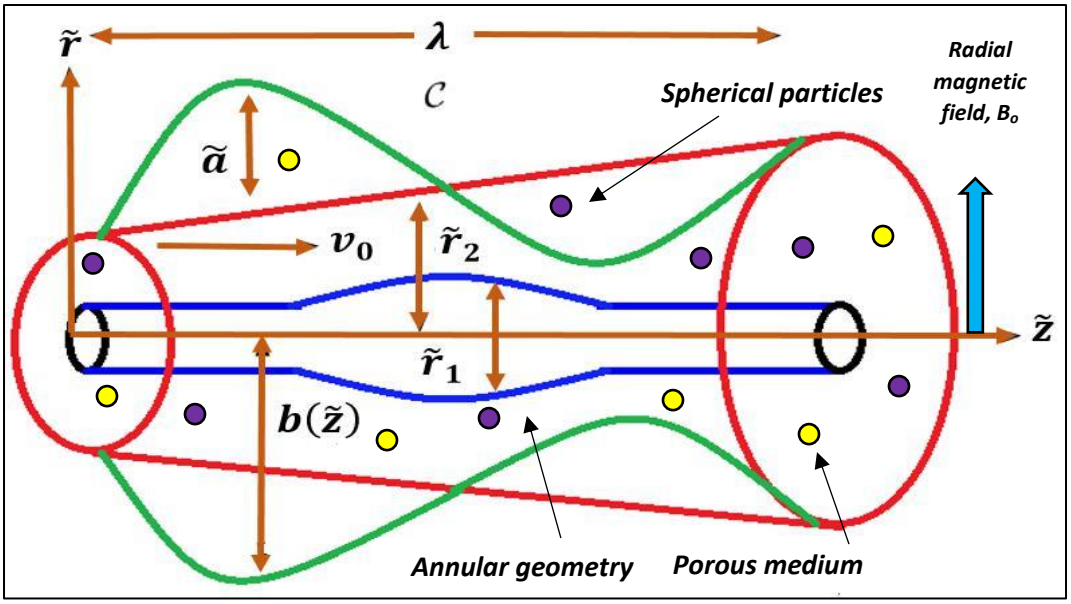

Fig. 1: Annular geometry of magnetic porous medium endoscopic model with coordinate system

Hall current is present in the magnetohydrodynamic regime and this generates a cross-flow [51-53].

In the above equation, c is the velocity of the peristaltic wave propagating along the inner and outer walls of the annulus, b_0 is a radius of the outer tube inlet, $\mathbf{K}$ is constant (its magnitude is a function of the length of the annulus), $\tilde{a}$ is amplitude of the peristaltic wave, $b(\tilde{z})$ is radius of the outer tube, λ is a wavelength, a is an inner tube radius that defines the clot axial location, $f\left(\tilde{z},t\right)$ the arbitrary shape along the axial direction that can be selected through a suitable choice, and $\tilde{t}$ is a time. The governing equations for the annular magnetized peristaltic two-phase Prandtl suspension flow may be summarized as follows:

(i) Fluid phase

$$(1-C)\frac{\partial \tilde{U}_f}{\partial \tilde{r}} = -(1-C)\frac{\partial \tilde{U}_f}{\partial \tilde{z}} - (1-C)\frac{\tilde{V}_f}{\tilde{r}}, \tag{3}$$

$$0 = \mu_s\left(\tilde{r}^{-1}\frac{\partial}{\partial \tilde{r}}\tilde{r}\tau_{\tilde{r}\tilde{r}} + \frac{\partial}{\partial \tilde{z}}\tau_{\tilde{r}\tilde{z}} - \frac{\tau_{\theta\theta}}{\tilde{r}}\right)(1-C) + SC(\tilde{V}_p - \tilde{V}_f) - (1-C)\frac{\partial \tilde{P}}{\partial \tilde{r}}, \tag{4}$$

$$0 = \mu_s(1-C)\left(\tilde{r}^{-1}\frac{\partial}{\partial \tilde{r}}\tilde{r}\tau_{\tilde{r}\tilde{z}} + \frac{\partial}{\partial \tilde{z}}\tau_{\tilde{z}\tilde{z}}\right) + SC(\tilde{U}_p - \tilde{U}_f) + \mathbf{J}\times\mathbf{B} - \frac{\mu_s}{K}u_f - (1-C)\frac{\partial \tilde{P}}{\partial \tilde{z}}. \tag{5}$$

(ii) Particulate phase

$$C\frac{\partial \tilde{V}_p}{\partial \tilde{r}} + C\frac{\partial \tilde{U}_p}{\partial \tilde{z}} + C\frac{\tilde{V}_p}{\tilde{r}} = 0, \tag{6}$$

$$0 = SC(-\tilde{V}_p + \tilde{V}_f) - C\frac{\partial \tilde{P}}{\partial \tilde{r}}, \tag{7}$$

$$0 = SC(-\tilde{U}_p + \tilde{U}_f) - C\frac{\partial \tilde{P}}{\partial \tilde{z}}, \tag{8}$$

The *Prandtl fluid stress tensor* is defined as [54]:

$$\tau = \frac{\bar{A}\sin^{-1}\left[\frac{1}{C'}\left(\left(\frac{\partial \tilde{V}_f}{\partial \tilde{z}}\right)^2 + \left(\frac{\partial \tilde{U}_f}{\partial \tilde{r}}\right)^2\right)^{1/2}\right]}{\sqrt{\left(\frac{\partial \tilde{V}_f}{\partial \tilde{z}}\right)^2 + \left(\frac{\partial \tilde{U}_f}{\partial \tilde{r}}\right)^2}}\frac{\partial \tilde{U}_f}{\partial \tilde{r}}, \tag{9}$$

Following Bhatti *et al.* [40] and Hayat *et al*. [45] we have:

$$\tilde{m} = \frac{7}{10}\exp\{\frac{1107}{\tilde{T}}\exp(-1.69C) + 2.49C\},$$
$$\tilde{\lambda}(C) = (2-3C)^{-2}\left[4 + 3C + \sqrt{8C - 3C^2}\right], \tag{10}$$
$$\mu_s = \frac{\mu_0}{1-\tilde{m}C}, \mathbf{J} = \sigma\left[\mathbf{E} + \mathbf{V}\times\mathbf{B}_0 - \frac{\mathbf{J}\times\mathbf{B}_0}{\mathbf{e}_n}\right], S = \frac{9}{2}\frac{\mu_0}{B_0^2}\tilde{\lambda}(C),$$

The corresponding boundary conditions are

$$\tilde{U}_f(\tilde{r}_1) = cv_0, \text{at } \tilde{r} = \tilde{r}_1, \tag{11a}$$

$$\tilde{U}_f\left(\tilde{r}_2\right)=0,\ \text{at}\ \tilde{r}=\tilde{r}_2, \tag{11b}$$

Where $\tilde{U}_f$ and $\tilde{U}_p$ are the particle and fluid phase velocities, B_0 is the radius of a spherical particle suspended in the biofluid, C is a particle volume fraction, μ_s is the apparent (effective) viscosity, S is a drag coefficient, $\tilde{T}$ is a temperature (measured in Kelvin), $\mathbf{B}_0$ is a applied radial magnetic field, μ_0 is the biofluid dynamic viscosity, $\mathbf{J}$ is a current density, σ is biofluid electrical conductivity, $\mathbf{V}$ is the velocity vector of the biofluid, $\boldsymbol{e}$ is an electron charge and n is the number of density electrons (associated with the Hall current effect), respectively. The conservation equations are normalized via the following non-dimensional variables:

$$\begin{aligned}
&rb_0=\tilde{r},z\lambda=\tilde{z},u_{f,p}=\frac{\tilde{U}_{f,p}}{c},v_{f,p}=\frac{\lambda\tilde{V}_{f,p}}{b_0c},t=\frac{\tilde{t}c}{\lambda},p=\frac{b_0^2}{\lambda\mu_0c}\tilde{P},\bar{\mu}=\frac{\mu_s}{\mu_0},v_0=\frac{\tilde{v}_0}{c},\\
&r_1=\frac{\tilde{r}_1}{b_0},r_2=\frac{\tilde{r}_2}{b_0},\varphi=\frac{\tilde{a}}{b_0},\bar{\delta}=\frac{b_0}{\lambda},N_1=\frac{CSb_0^2}{(1-C)\mu_0},N_2=\frac{Sb_0^2}{\mu_0},M=\frac{\sigma\mathbf{B}_0^2b_0^2}{\mu_0},\\
&k=\frac{K}{b_0},\alpha=\frac{\bar{A}}{\mu_0C'},\beta=\frac{\bar{A}c^2}{6b_0^2\mu_0C'^3},
\end{aligned} \tag{12}$$

The parameters in Eqn. (12) denote respectively the normalized (dimensionless) versions of radial coordinate, axial coordinate, radial components of fluid and particle velocities, axial components of fluid and particle velocity components, time, pressure, viscosity, wall lateral mass flux velocity, inner tube radius, outer tube radius, amplitude ratio, interphase momentum transfer coefficients for the fluid and particle phases, magnetohydrodynamic body force parameter (Hartmann number), Darcy number (permeability parameter), and Prandtl rheological material constants. Taking the approximation of a creeping flow regime with long wavelength and using Eq. (12) in Eq. (3) to Eq. (9), we obtain the reduced conservation equations:

$$\frac{\partial p}{\partial r}=0, \tag{13}$$

$$\frac{\partial p}{\partial z}=\bar{\mu}r^{-1}\frac{\partial}{\partial r}\left[r\alpha\frac{\partial u_f}{\partial r}+\beta r\left(\frac{\partial u_f}{\partial r}\right)^3\right]-\frac{M^2}{1+m^2}u_f-\frac{1}{k}u_f-N_1\left(u_p-u_f\right), \tag{14}$$

$$u_p=u_f-\frac{1}{N_2}\frac{\partial p}{\partial z}. \tag{15}$$

It emerges that p does not depend on r (see Eq. (14)). The respective boundary conditions on the inner and outer walls of the annular zone are:

$$u_f(r_1) = v_0, r_1 = a(z) = a_0 + \delta e^{-\pi^2 (z - z_d - 0.5)^2}, \tag{16}$$

$$u_f(r_2) = 0, r_2 = 1 + \frac{\lambda \mathbf{K} z}{b_0} + \varphi \sin(2\pi x - 2\pi t). \tag{17}$$

In the above equations, δ is the maximum height of clot, z_d describes the axial displacement of a clot and m is the Hall parameter.

3. ANALYTICAL SOLUTION WITH HPM

The series solution of Eq. (14) can be obtained using homotopy perturbation method (HPM). This is a semi-numerical/analytical method introduced by He [55]. It has found immense popularity in recent years and has been implemented successfully in peristaltic flows and nonlinear mechanics extensively- see [56-58]. The homotopy for Eq. (14) is defined as:

$$\mathbf{H}(w, \hat{\theta}) = \left(1 - \hat{\theta}\right)\left[\hat{L}(w) - \hat{L}(\hat{w}_0)\right] + \hat{\theta}\left[\begin{array}{l} L(w) + \frac{3\beta}{\alpha}\left(\frac{\partial w}{\partial r}\right)^2\left(\frac{\partial^2 w}{\partial r^2}\right) + \frac{\beta}{r\alpha}\left(\frac{\partial w}{\partial r}\right)^3 \\ -\frac{M^2}{(1+m^2)\alpha\bar{\mu}} w - \frac{1}{\alpha k} w - \frac{1}{\alpha}\frac{dp}{dz} \end{array}\right], \tag{18}$$

where $\hat{\theta}$ denotes the embedding parameter. The following linear operator is selected:

$$L = \frac{\partial^2}{\partial r^2} + \frac{1}{r}\frac{\partial}{\partial r}. \tag{19}$$

An initial guess is selected of the following form:

$$\tilde{w}_0 = v_0 \{\log r_1 - \log r_2\}^{-1} \log r - v_0 \{\log r_1 - \log r_2\}^{-1} \log r_2. \tag{20}$$

Defining the following expansion:

$$w(r,z) = w_0 + \hat{\theta} w_1 + \hat{\theta}^2 w_2 + \cdots. \tag{21}$$

Now, using Eq. (21) in Eq. (18), we obtained a set of differential equations along with the corresponding boundary conditions. Using a key property of He's homotopy perturbation method, we obtain the solution as $\hat{\theta} \to 1$, i.e.

$$u_f(r,z) = w(r,z) = w_0 + w_1 + w_2 + \cdots. \tag{22}$$

The solution for *velocity profile* are obtained as

$$u_f = \frac{C_0 + C_1 r^2 + C_2 r^4 + C_3 r^2 \log r + C_4 r^4 \log r + C_5 \log r}{C_6 r^2}, \tag{23}$$

and

$$u_p = \frac{C_0 + C_1 r^2 + C_2 r^4 + C_3 r^2 \log r + C_4 r^4 \log r + C_5 \log r}{C_6 r^2} - \frac{1}{N_2}\frac{dp}{dz}. \tag{24}$$

The constants in the above equations can be obtained using **MATHEMATICA** symbolic software. The *instantaneous volumetric flow rate* for the particulate and fluid phase is given by:

$$Q(z,t) = 2\pi(1-C)\int_{r_1}^{r_2} r u_f \,\mathrm{d}r + 2\pi C \int_{r_1}^{r_2} r u_p \,\mathrm{d}r. \tag{25}$$

The *pressure elevation* and *friction forces (on the outer and inner tube)* along the *whole length of annulus* are computed according to the following formulae:

$$\Delta p_L(t) = \int_0^{L/\lambda} \frac{dp}{dz}\,\mathrm{d}z, \tag{26}$$

$$\Delta f_O(t) = \int_0^{L/\lambda} r_2^2 \left(-\frac{dp}{dz}\right)\mathrm{d}z, \tag{27}$$

$$\Delta f_I(t) = \int_0^{L/\lambda} r_1^2 \left(-\frac{dp}{dz} \right) \mathrm{d}z. \tag{28}$$

In the analytical evaluations (plotted in section 5), we have considered the *volumetric flow rate* which is periodic in $(z-t)$ of the following form:

$$\frac{\bar{Q}}{\pi} = \frac{Q(z,t)}{\pi} + \frac{\varphi^2}{2} - 2\varphi \sin 2\pi(z-t) - \frac{2\mathbf{K}\lambda z}{b_0}\varphi \sin 2\pi(z-t) - \varphi^2 \sin^2 2\pi(z-t). \tag{29}$$

In the above equation, the following parameter values [32-34, 41-45] i.e. $b_0 = 1.25\mathrm{cm}, C = 0-0.6, L = \lambda = 8.01\mathrm{cm}, \mathbf{K} = 3b_0/\lambda$ have been utilized to calculate the expression of friction forces and pressure rise. We considered this form of $Q(z,t)$ due to the fact that for a constant value of $Q(z,t)$, pressure rise shows negative values and as a result no pumping action is observed.

4. VALIDATION WITH MAPLE QUADRATURE

The linear dimensionless two-point moving boundary value problem (BVP) i.e. eqns. (13)-(15) under boundary conditions (16) and (17) are easily solved using Runge–Kutta–Merson numerical quadrature to yield *fluid velocity and particle phase velocity*. The pressure difference and friction forces are then subsequently computed with Eqns. (26)-(28). The computations are executed in **MAPLE17** software (RK45 algorithm). This approach has been extensively implemented recently in non-Newtonian nanofluid flows [59], magnetohydrodynamics [60] and biological hydrodynamics [61]. The robustness and stability of this numerical method is therefore well established - it is highly adaptive since it adjusts the quantity and location of grid points during iteration and thereby constrains the local error within acceptable specified bounds. In the current problem, the complex wall boundary conditions given in Eqns. (16, 17) are easily accommodated. The stepping formulae, although designed for nonlinear problems, are even more efficient for any order of linear differential equation and are summarized below [59-61]:

$$k_0 = f(x_i, y_i), \tag{30}$$

$$k_1 = f\left(x_i + \frac{1}{4}h, y_i + \frac{1}{4}hk_0\right), \tag{31}$$

$$k_2 = f\left(x_i + \frac{3}{8}h, y_i + \left(\frac{3}{32}k_0 + \frac{9}{32}k_1\right)h\right), \tag{32}$$

$$k_3 = f\left(x_i + \frac{12}{13}h, y_i + \left(\frac{1932}{2197}k_0 - \frac{7200}{2197}k_1 + \frac{7296}{2197}k_2\right)h\right), \tag{33}$$

$$k_4 = f\left(x_i + h, y_i + \left(\frac{439}{216}k_0 - 8k_1 + \frac{3860}{513}k_2 - \frac{845}{4104}k_3\right)h\right), \tag{34}$$

$$k_5 = f\left(x_i + \frac{1}{2}h, y_i + \left(-\frac{8}{27}k_0 + 2k_1 - \frac{3544}{2565}k_2 + \frac{1859}{4104}k_3 - \frac{11}{40}k_4\right)h\right), \tag{35}$$

$$y_{i+1} = y_i + \left(\frac{25}{216}k_0 + \frac{1408}{2565}k_2 + \frac{2197}{4104}k_3 - \frac{1}{5}k_4\right)h, \tag{36}$$

$$z_{i+1} = z_i + \left(\frac{16}{135}k_0 + \frac{6656}{12825}k_2 + \frac{28561}{56430}k_3 - \frac{9}{50}k_4 + \frac{2}{55}k_5\right)h, \tag{37}$$

Here y denotes fourth-order Runge-Kutta phase and z is the fifth-order Runge-Kutta phase. An estimate of the error is achieved by subtracting the two values obtained. If the error exceeds a specified threshold, the results can be re-calculated using a smaller step size. The approach to estimating the new step size is shown below:

$$h_{\text{new}} = h_{\text{old}}\left(\frac{\varepsilon h_{\text{old}}}{2\left|z_{i+1} - y_{i+1}\right|}\right)^{1/4} \tag{37}$$

A comparison of the analytical and **MAPLE17** numerical quadrature solutions (blue dots) is documented in **Fig. 2** for pressure rise profile with variation in Hall current parameter and Prandtl first material constant over time. The *comparison case* is for $m = 0.1$, $\alpha = 3$. Data is based on real blood properties under magnetic field and extracted from Mekheimer *et al.* [32], Gad *et al.* [33], Ramesh *et al.* [41] and Hayat *et al.* [45].

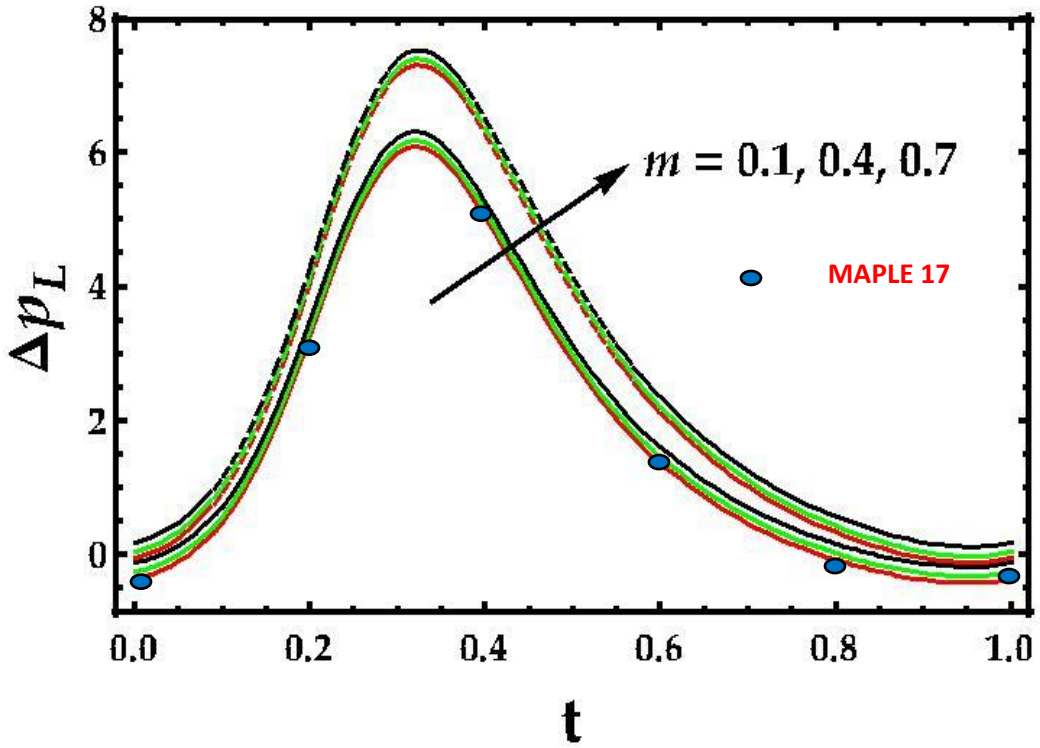

Fig. 2: Pressure rise for multiple values of m and α (*Dashed line:* $\alpha = 4$*; Solid line:* $\alpha = 3$)

Excellent correlation is achieved. Confidence in the present analytical HPM solutions is therefore high. Maple quadrature is of comparable accuracy to many other sophisticated semi-numerical methods including homotopy analysis methods (HAM), Adomian decomposition methods (ADM), spectral collocation Chebyschev polynomial methods and variational iterative methods (VIMs) which accurately compute series solution, although Maple quadrature is less algebraically rigorous and can be applied directly for all types of differential and integral equations, linear or nonlinear, homogeneous or inhomogeneous, with constant coefficients or with variable coefficients. Another important advantage is that the method is capable of greatly reducing the size of computation work while still maintaining high accuracy of the numerical solution [59-61]. It is also worth mentioning here that, the current model reduces to that studied by Mekheimer *et al.*

[32] by taking $M = 0, \alpha = 1, \beta = 0, k \to \infty, \delta = 0$.

5. RESULTS AND DISCUSSION

In this section, the HPM theoretical results are presented graphically as transient distributions. A parametric analysis of the key parameters on pressure elevation and friction forces is conducted. The symbolic software **Mathematica** has been utilized to evaluate the expressions for pressure rise (Δp_L), friction force on the outer tube surface (Δf_O) and friction force on the inner tube surface (Δf_I). In particular, the impact of all the pertinent parameters such as clot height (δ), particle volume fraction (C), Prandtl first and second rheological material parameters (α, β), Hartmann (magnetohydrodynamic body force) number (M), medium permeability parameter i.e. Darcy number (k) and Hall parameter (m) is addressed.

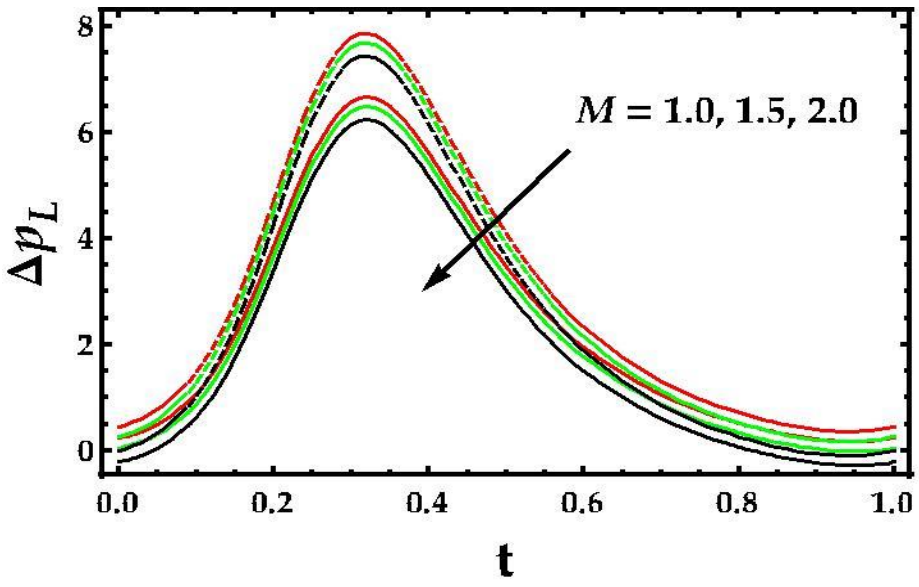

Fig. 3: Transient pressure rise with variation in M and β .[Dashed line: β = 0:5; Solid line: β = 0:1]

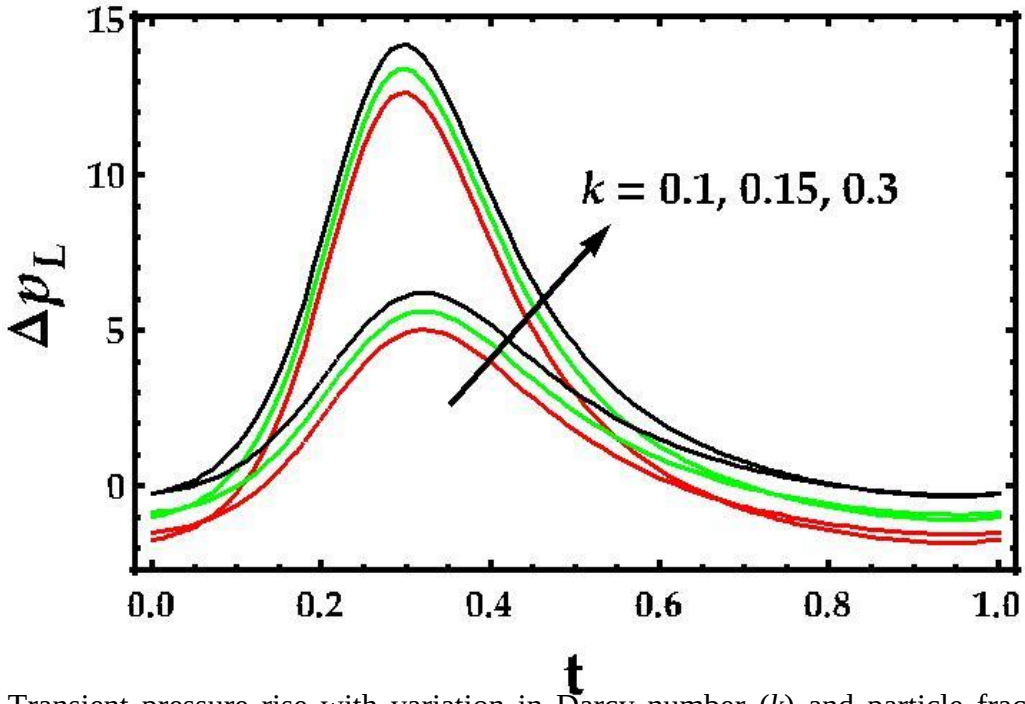

Fig. 4: Transient pressure rise with variation in Darcy number (k) and particle fraction (C). [Dashed line: C = 0:1; Solid line: C = 0]

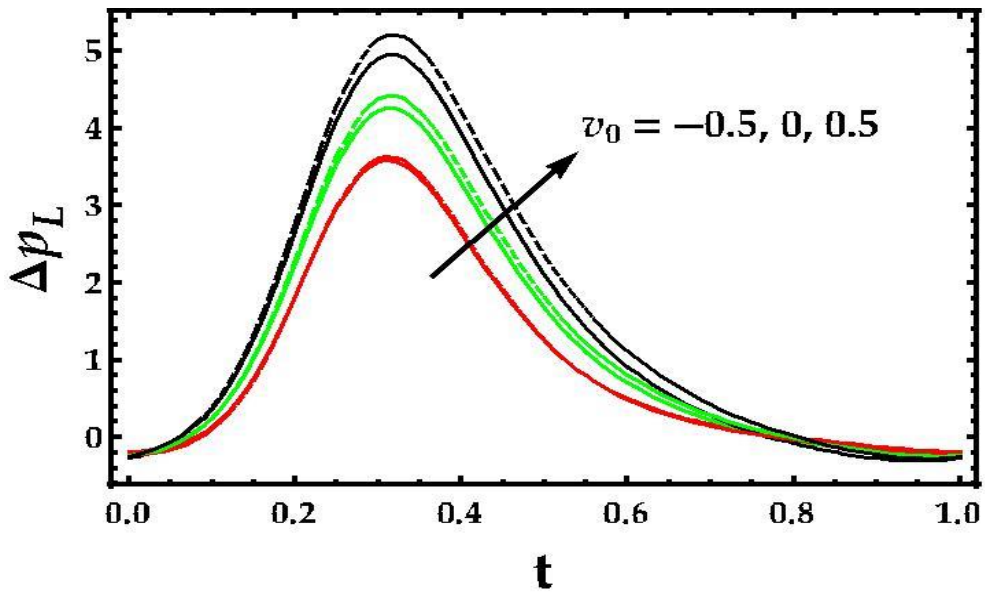

Fig. 5: Pressure rise for multiple values of v_0 and δ. [Dashed line: δ = 0:1; Solid line: δ = 0]

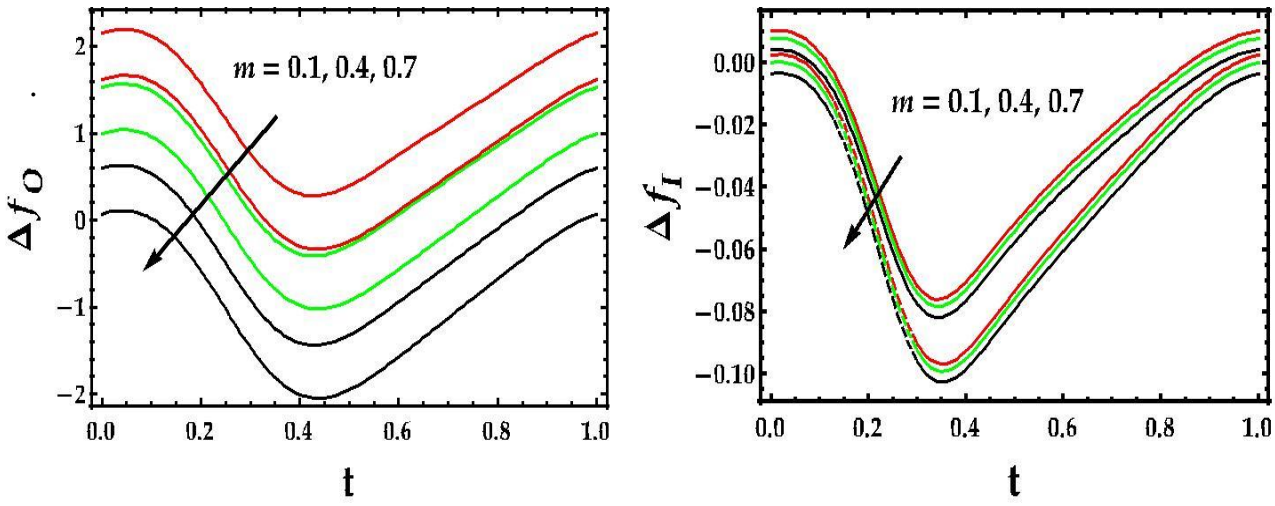

(a)Outer tube (b)Inner tube

Fig. 6: Friction forces for multiple values of m and α . [Dashed line: α = 4; Solid line: α = 3]

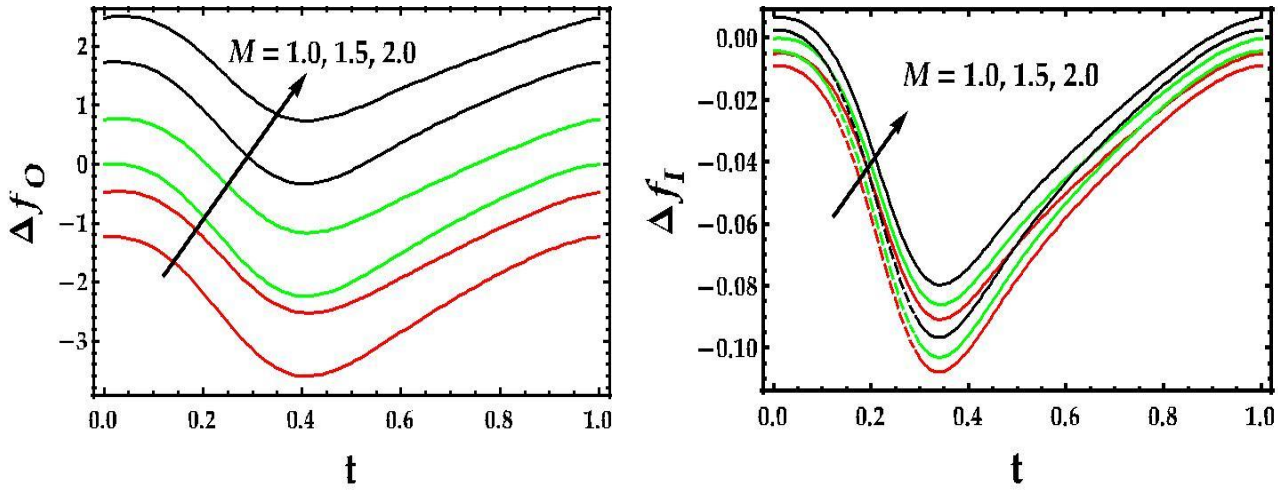

(a)Outer tube (b)Inner tube

Fig. 7: Friction forces for multiple values of M and β . [Dashed line: β = 0:5; Solid line: β = 0:1]

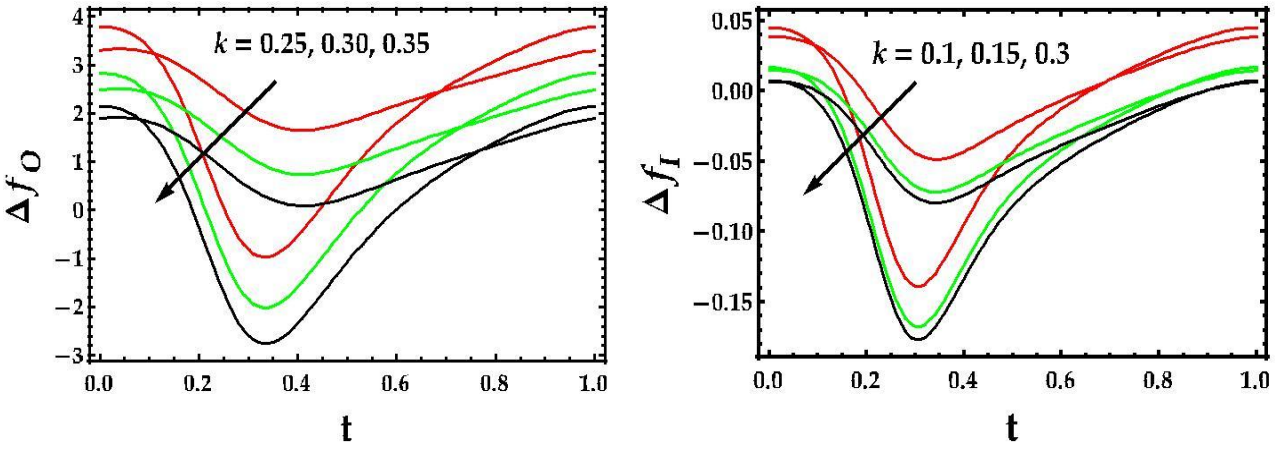

(a)Outer tube (b)Inner tube

Fig. 8: Friction forces for multiple values of k and C. [Dashed line: C = 0:1; Solid line: C = 0]

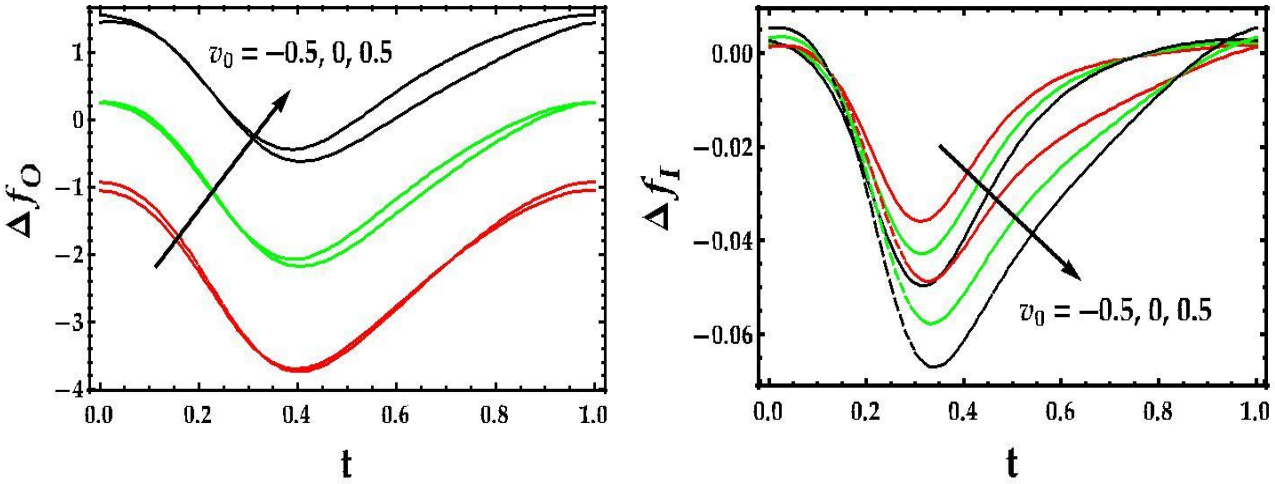

(a)Outer tube (b)Inner tube

Fig. 9: Friction forces for multiple values of v_0 and δ . [Dashed line: δ = 0:1; Solid line: δ = 0]

Furthermore, the results for a *Newtonian fluid* may be retrieved by taking $\alpha = 1, \beta = 0$ (see Eq. (14)). Hence the first Prandtl material constant must be unity and the second Prandtl material constant must be zero to obtain the *Newtonian viscous* case.

Fig. (2) shows the behavior of dimensionless pressure versus time for different values of Hall parameter (m) and first Prantl rheological parameter (α). We can observe that pressure rise increases with the increment in hall parameter m. However, in this figure, we can also see that when the fluid parameter α increases then the pressure rise also increases significantly. The Hall parameter arises in the magnetic body force term, -[$M^2/(1+m^2)$]u_f associated with the fluid phase longitudinal (axial) velocity in the normalized axial momentum Eqn. (13). There is an inverse quadratic relationship between Hall current parameter and the overall Lorentzian drag. The ionized biofluid contains electrons which make cyclotron orbits between the collisions and are diverted in a direction mutually perpendicular to the magnetic and electric field directions. Thus, if an electric field is applied perpendicular to the magnetic field then whole current will not pass along the electric field. This complex phenomenon of flow of the electric current across an electric field with an orthogonal magnetic field constitutes the *Hall effect*, and the associated electrical current is known as the *Hall current*. The enhancing influence on pressure rise implies that the primary (axial flow) is retarded by Hall current (there is generally an inverse relationship between pressure and velocity field). The Prandtl first rheological parameter, $\alpha = A/\mu_0 C'$ is inversely proportional to dynamic viscosity for constant values of the other parameters. It is coupled to the radial velocity gradient term, $\partial u_f/\partial r$ in the dimensionless momentum Eqn. (13), and clearly greater values of this rheological parameter will serve to decelerate the longitudinal flow. This will manifest in an elevation in pressure difference, Δp_L, as observed in **fig.2**. Similar findings have been reported in Riaz *et al.* [54]. We further note that in the present analysis, Ohmic (Joule) dissipation and magnetic induction effects are negated i.e. the magnetic field is not distorted by fluid vorticity owing to sufficiently low magnetic Reynolds numbers in the regime, although this can be addressed in future studies.

Fig. (3) illustrates the evolution in dimensionless pressure rise Δp_L with time for various values of the Hartmann number (M) and the Prandtl second rheological fluid parameter (β). As noted earlier the periodic nature of the peristaltic pumping is clearly captured in the undulatory profile with time elapse. Increasing Hartmann number (M) causes a marked reduction in a pressure rise. When the

fluid is non-Newtonian $\beta \neq 0$. For lower values of this parameter, pressure rise is reduced, however when this rheological parameter $\beta > 0$ increases, there is a significant elevation in the pressure rise. The effect is more significant than for the Prandtl first rheological parameter (fig. 2) and this is probably attributable to the coupling of the Prandtl second rheological fluid parameter (β) with a cubic velocity gradient term in Eqn. (13) i.e. $(\partial u_f / \partial r)^3$ in the modified shear contributions. This term is completely absent when the fluid is Newtonian ($\beta \rightarrow 0$) whereas the first shear term, $r\alpha \partial u_f / \partial r$ merely contracts to $r \partial u_f / \partial r$ *(since* $\alpha \rightarrow 1$ *for Newtonian fluids).* Overall the pressure difference is minimized for the case $M = 2$ (for which Lorentz magnetic drag is double the magnitude of the viscous force) and $\beta = 0.1$. The general trends are in good agreement also with Akbar [62], Yıldırım and Sezer [63] and Hayat *et al.* [64].

Fig. (4) visualizes the collective influence of an increment in the Darcy number, k (i.e. permeability parameter) and particle fraction (C) over time. The Darcian porous medium resistance (produced by solid fibers in the regime e.g. blockages, debris, clusters etc) is inversely proportional to the Darcy number, as embodied in the term $-(1/k)\, u_f$ in Eqn. (13). With increasing Darcy number, the solid matrix fibers progressively decrease and the permeability increases, as elaborated by Bég *et al*. [65], Bejan [66] and Scheidegger [67]. The Darcy impedance is thereby reduced. In the limit, as $k \rightarrow \infty$, *the* solid matrix fibers vanish completely and effectively therefore the regime becomes purely viscous electrically-conducting Prandtl fluid. With increasing particle fraction, C, from 0 (single phase flow case) to 0.1, the inter-phase momentum coefficient N_1 is invoked so that the fluid-particle relative velocity term, $-N_1(u_p - u_f)$ is then activated in Eqn. (13). This results in greater impedance to the pressure development and manifests in a decrease in pressure difference in fig. 4. The presence of two-phase flow therefore has a non-trivial influence on one of the key performance criteria in peristaltic endoscopic pumps i.e. pressure field. Neglecting the particle phase results in an over-prediction in pressure elevation which is undesirable for medical applications. The oscillatory (sinusoidal) distribution of pressure rise with time is clearly reflected in fig. 4 and characterizes the sinusoidal peristaltic wave propagation along the annulus walls.

Fig. (5) presents the transient evolution in pressure rise along the length of the endoscopic annulus with a variation in the height of clot, δ and wall transpiration velocity, v_0. It can be observed from this figure that pressure rise increases with the increment in height of clot, δ. Moreover, the results for non-clotted endoscope can be recovered by taking $\delta = 0$. This follows logically since the

presence of a clot adds a significant impedance to the flow and strongly alters vorticity in the vicinity of the clot. The pumping is therefore inhibited and pressure elevation along the length of the duct is adversely affected. Furthermore, with suction at the wall (i.e. removal of Prandtl fluid from the annular region to the external space) the longitudinal (axial) flow will be impeded (deceleration) and pressure rise will also be reduced. The converse effect is generated with wall injection (blowing of Prandtl fluid into the annular region), i.e. pressure rise is boosted. The case of solid walls corresponds to $v_0=0$ i.e. zero lateral mass flux and naturally falls in between the blowing and suction scenarios. Inspection of Fig. (2) and Fig. (5), also reveals that maximum pressure is attained at $t = 0.3$.

Fig. (6a,b) present the transient profiles for friction force elevation on the inner tube (Δf_I) and outer tube (Δf_O) of the annulus, for different values of Hall parameter (m) and Prandtl first rheological parameter (α). An increase in the Hall parameter strongly reduces both friction force increments i.e. induces significant deceleration on both the outer and inner tube surfaces. However, there is no tangible modification in the friction force increments with an increase in Prandtl behaviors remains similar for fluid parameter, α. Rheology of the Prandtl fluid will affect the velocity distributions across the annular cross-section. However, at the walls it will exert a trivial effect. It is also pertinent to note that the magnitudes of the outer tube friction are significantly higher (an order of magnitude) compared with the inner tube friction forces.

Fig. (7a,b) illustrates the evolution in friction force elevation on the inner tube (Δf_I) and outer tube (Δf_O) of the annulus, for different values of Hartmann magnetic number (*M*) and Prandtl second rheological parameter (β). A significant enhancement in outer tube friction force and a weaker elevation in inner tube friction force accompanies an increase in Hartmann number (M) indicating that flow is significantly influenced at the walls of the annulus. Conversely the opposite behavior is induced in the friction force on the inner tube with an increase in the second rheological parameter (β) i.e. friction force is decreased. However, no marked alteration is induced in the outer tube friction force.

Fig. (8a, b) presents the distributions for friction force elevation on the inner tube (Δf_I) and outer tube (Δf_O) of the annulus, with different values of Darcy number (*k*) and particle volume fraction (*C*). With an increase in Darcy number there is a significant reduction in both outer and inner friction forces and again the periodic nature of the peristaltic flow is amply demonstrated. When

the particle volume fraction increases from C = 0 (single phase flow) to C = 0.1 (two-phase suspension) there is no tangible modification in the magnitude of the friction forces on either surface of the annular tube.

Fig. (9) depicts the evolution in friction force elevation on the inner tube (Δf_I) and the outer tube (Δf_O) of the endoscopic annulus, for different values of clot height (δ) and wall transpiration (v_0). The presence of a clot (thrombosis, obstruction etc) generates greater resistance to the shearing (friction) forces especially for the inner tube and decreases values. The effect is simulated via the complex boundary condition (15), viz, $u_f(r_1) = v_0, r_1 = a(z) = a_0 + \delta e^{-\pi^2(z-z_d-0.5)^2}$, and is significant. Friction force for the outer tube increases with wall injection (v_0 >0) and reduces with wall suction (v_0 <0) whereas the contrary response is computed for the friction force on the inner tube i.e. a reduction is induced with wall injection whereas an elevation is caused with wall suction. Generally, as with other plots, friction force on the outer tube attains substantially greater magnitude as compared to friction force on the inner tube surface.

6. CONCLUSIONS

As a simulation of *more realistic obstructed magnetic endoscope fluid dynamics*, a mathematical model has been developed in this article for the *influence of a clot in peristaltic magnetohydrodynamic non-Newtonian two-phase (fluid-particle suspension) through an annular geometry containing a homogenous, isotropic high-permeability porous medium under the action of a radial static magnetic field*. Hall current magneto-dynamic effect has been incorporated in the model and the classical Darcy model for viscous-dominated flow has been used. The rheology of the two-phase biofluid is analyzed with the Prandtl two-parameter model. The mathematical problem is reduced in complexity via lubrication approximations, normalized with appropriate transformations and the resulting boundary value problem is solved with He's homotopy perturbation method. Thereafter fluid and particle velocity solutions are computed with **Mathematica** symbolic software. The analytical solutions are verified with **Maple17** numerical quadrature. The present computations have illustrated the variation of key flow characteristics with time and have shown that:

i. Pressure rise increases with increasing height of the clot.

ii. Pressure rise increases with Prandtl's first and second rheological material parameters and

also Darcy number (permeability parameter).

iii. Pressure rise decreases markedly for higher values of particle volume fraction and Hartmann (magnetic body force) number.

iv. Friction forces on the inner and outer tube surfaces of the annular region in the magnetic endoscope generally increase with an increment in the height of the clot.

v. Friction forces increase due to an increment in particle volume fraction, with the opposite behavior computed with increasing Prandtl rheological material parameters.

vi. Friction forces are reduced with Hall current parameter and Darcy number (permeability parameter).

vii. The general mathematical model developed can be reduced to the *Newtonian, electrically non-conducting case* (as considered in previous studies) by considering $\alpha = 1, \beta = 0.$ and $M = 0$ (vanishing Lorentz magnetic body force)

viii. The case of an unobstructed endoscope is retrieved by setting clot height to zero ($\delta = 0$).

ix. The inclusion of a *particle phase* results in *non-trivial modifications* to the pressure and friction force distributions in magnetic annular endoscopic hemodynamics and produces superior results to conventional *single-phase* models.

The current simulations have neglected heat and mass diffusion in peristaltic magnetic pumping which may arise via, for example, nano-doping of working fluids [67]. These will be considered in the future.

ACKNOWLEDGEMENTS

The authors wish to express their gratitude to the reviewers who highlighted important areas for improvement in this article.

REFERENCES

[1] C.C. Huang, S.H. Wang, Assessment of blood coagulation under various flow conditions with ultrasound backscattering, IEEE Trans. Biomed. Eng. 54 (2007) 2223-2230. https://doi.org/10.1109/TBME.2007.908334.

[2] H.L. Goldsmith and R. Skalak, Hemodynamics, Ann. Rev. Fluid Mech. 7 (1975) 213-247. https://doi.org/10.1146/annurev.fl.07.010175.001241.

[3] Y.C. Fung, Biomechanics: Circulation, Springer, New York, USA, 1997. https://doi.org/10.1007/978-1-4757-2696-1.

[4] G.H. Mostbeck, G.R. Caputo, C.B. Higgins, MR measurement of blood flow in the cardiovascular system, AJR. Am. J. Roentgenol. 159 (1992) 453-461. https://doi.org/10.2214/ajr.159.3.1503004

[5] F. Carpi, Magnetic capsule endoscopy: the future is around the corner, Expert Rev. Med. Devices 7 (2010) 161-164. https://doi.org/10.1586/erd.10.3.

[6] S. Schlag, B. Neu, P. Klare, S. Wagenpfeil, R. M. Schmid, S.V. Delius, Magnetic endoscope imaging in single-balloon enteroscopy, Dig. Endosc. 27 (2015) 465-470. https://doi.org/10.1111/den.12415.

[7] V.K. Sud, G.S. Sekhon, and R.K. Mishra, Pumping action on blood by a magnetic field, Bull. Math. Biol. 39 (1977) 385-390. https://doi.org/10.1007/BF02462917.

[8] S. Cheng, M.W. Olles, D.B. Olsen, Miniaturization of a magnetically levitated axial flow blood pump, J. Artif. Organs. 34, (2010) 807–815. https://doi.org/10.1111/j.1525-1594.2010.01077.x.

[9] D. Xia, A bionic artificial heart blood pump driven by permanent magnet located outside human body, IEEE Trans. Appl. Supercond. 22 (2012) 4401304–4401304. https://doi.org/10.1109/TASC.2011.2174582.

[10] A. Hilton and T. Geoff, Magnetic drive system for a new centrifugal rotary blood pump, J. Artif. Organs. 32 (2008) 772–777. https://doi.org/10.1111/j.1525-1594.2008.00629.x.

[11] D. D'Ambrosio, D. Giordano, Electromagnetic fluid dynamics for aerospace applications, J. thermophys. heat tr. 21 (2007) 284-302. https://doi.org/10.2514/1.24732.

[12] O. Anwar Bég and D. Tripathi, Peristaltic pumping of nanofluids, Modeling and Simulation Methods and Applications, (Eds.), Springer, Berlin, 2014, pp. 69-96. https://doi.org/10.1007/978-3-319-05657-9_4.

[13] M. Jaffrin and A.H. Shapiro, Peristaltic pumping, Ann. Rev. Fluid Mech. 3 (1971) 13-37. https://doi.org/10.1146/annurev.fl.03.010171.000305.

[14] T.D. Brown and T.K. Hung, Computational and experimental investigation of two-dimensional nonlinear peristaltic flow, J. Fluid Mech. 83 (1977) 249-273. https://doi.org/10.1017/S0022112077001189.

[15] A. M. Siddiqui, W. H. Schwarz, Peristaltic flow of a second-order fluid in tubes, J. Non-Newtonian Fluid Mech. 53 (1994) 257-284. https://doi.org/10.1016/0377-0257(94)85052-6a.

[16] K. Vajravelu, G. Radhakrishnamacharya, V. Radhakrishnamurty, Peristaltic flow and heat transfer in a vertical porous annulus, with long wave approximation, Int. J. Non-Linear Mech. 42 (2007) 754-759. https://doi.org/10.1016/j.ijnonlinmec.2007.02.014.

[17] N.S. Akbar, S. Nadeem, Peristaltic flow of a Phan-Thien-Tanner nanofluid in a diverging tube, Heat Transfer Asian Res. 41 (2012) 10-22. https://doi.org/10.1002/htj.20386.

[18] D. Tripathi, S. K. Pandey, S. Das, Peristaltic flow of viscoelastic fluid with fractional Maxwell model through a channel, Appl. Math. Comp. 215 (2010) 3645-3654. https://doi.org/10.1016/j.amc.2009.11.002.

[19] R. Ellahi, A. Riaz, S. Nadeem, M. Mushtaq, Series solutions of magnetohydrodynamic peristaltic flow of a Jeffrey fluid in eccentric cylinders, Appl. Math Inf. Sci. **7** (2013) 1441. https://doi.org/10.12785/amis/070424.

[20] S. Maiti, J.C. Misra, Peristaltic transport of a couple stress fluid: some applications to hemodynamics, J. Mech. Med. Biol. 12 (2012) 1250048. https://doi.org/10.1142/S0219519411004733.

[21] M.M. Bhatti, A. Zeeshan, Heat and mass transfer analysis on peristaltic flow of particle-fluid suspension with slip effects, J. Mech. Med. Biol. 17 (2012) 1750028. https://doi.org/10.1142/S0219519417500282.

[22] A. Zeeshan, N. Ijaz, M.M. Bhatti, A.B. Mann, Mathematical study of peristaltic propulsion of solid–liquid multiphase flow with a biorheological fluid as the base fluid in a duct, Chin. J. Phys. 55 (2017) 1596-1604. https://doi.org/10.1016/j.cjph.2017.05.020.

[23] S.Hina, M. Mustafa, T. Hayat, and A. Alsaedi, Peristaltic flow of couple-stress fluid with heat and mass transfer: An application in biomedicine, J. Mech. Med. Biol. 15 (2015) 1550042. https://doi.org/10.1142/S0219519415300057.

[24] M.M. Bhatti, A. Zeeshan, and R. Ellahi, Study of heat transfer with nonlinear thermal radiation on sinusoidal motion of magnetic solid particles in a dusty fluid, J. Theor. Appl. Mech. 46 (2016) 75-94. https://doi.org/10.1515/jtam-2016-0017.

[25] P. Nagarani, A. Lewis, Peristaltic flow of a Casson fluid in an annulus, Korea-Aust. Rheol. J. 24 (2012) 1-9. https://doi.org/10.1007/s13367-012-0001-6.

[26] C. Vlachopoulos, M. O'Rourke, W.W. Nichols, McDonald's blood flow in arteries: theoretical, experimental and clinical principles, sixth ed., CRC press, London, 2011. https://doi.org/10.1201/b13568.

[27] B.M. Johnston, P.R. Johnston, S. Corney, D. Kilpatrick, Non-Newtonian blood flow in human right coronary arteries: steady state simulations, J. Biomech. 37 (2004) 709-720. https://doi.org/10.1016/j.jbiomech.2003.09.016.

[28] J. Li, E.S. Barjuei, G. Ciuti, Y. Hao, P. Zhang, A. Menciassi, Q. Huang, Paolo Dario, Magnetically-driven medical robots: An analytical magnetic model for endoscopic capsules design, J. Magn. Magn. Mater. 452 (2018) 278-287. https://doi.org/10.1016/j.jmmm.2017.12.085.

[29] Kh. S. Mekheimer, Elsayed F. El Shehawey, A.M. Elaw, Peristaltic motion of a particle-fluid suspension in a planar channel, Int. J. Theor. Phys. 37 (1998) 2895-2920. https://doi.org/10.1023/A:1026657629065.

[30] C. Kleinstreuer, P.W. Longest, Z. Zhang, Theory of two-phase biofluid flow dynamics and selected applications, In ASME 2004 Heat Transfer/Fluids Engineering Summer Conference, pp. 741-750. American Society of Mechanical Engineers, 2004. https://doi.org/10.1115/HT-FED2004-56560

[31] J. Jung, Robert W. Lyczkowski, Chandrakant B. Panchal, and Ahmed Hassanein, Multiphase hemodynamic simulation of pulsatile flow in a coronary artery, J. Biomech. 39 (2006) 2064-2073. https://doi.org/10.1016/j.jbiomech.2005.06.023.

[32] Kh.S. Mekheimer, Y. Abd Elmaboud, Peristaltic transport of a particle-fluid suspension through a uniform and non-uniform annulus, Appl. Bio. Biomech. 5 (2008) 47-57. http://dx.doi.org/10.1080/11762320802376183.

[33] N.S. Gad, Effect of Hall currents on interaction of pulsatile and peristaltic transport induced flows of a particle-fluid suspension, Appl. Math. Comput. 217 (2011) 4313-4320. https://doi.org/10.1016/j.amc.2010.08.016.

[34] T.A. Bég, M.M. Rashidi, O. Anwar Bég and N. Rahimzadeh, Differential transform semi-numerical simulation of biofluid-particle suspension flow and heat transfer in non-Darcian porous media, Comput. Methods Biomech. Biomed. Engin. 16 (2013) 896-907. https://doi.org/10.1080/10255842.2011.643470.

[35] M.M. Bhatti, A. Zeeshan, N. Ijaz, Slip effects and endoscopy analysis on blood flow of particle-fluid suspension induced by peristaltic wave, J. Mol. Liq. 218 (2016) 240-245. https://doi.org/10.1016/j.molliq.2016.02.066.

[36] O. Anwar Bég, M.M. Rashidi, N. Rahimzadeh, T.A. Bég and T.K. Hung, Homotopy simulation of two-phase thermo-hemodynamic filtration in a high permeability blood purification device, J. Mech. Med. Biol. 13 (2013) 1350066. https://doi.org/10.1142/S0219519413500668.

[37] O. Anwar Bég, B. Vasu, T. Sochi and V.R. Prasad, Keller box and smoothed particle hydrodynamic numerical simulation of two-phase transport in blood purification auto-transfusion dialysis hybrid device with Stokes and Darcy number effects, Journal of Advanced Biotechnology and Bioengineering, 1 (2013) 80-100. https://doi.org/10.12970/2311-1755.2013.01.02.4.

[38] S. Nadeem, A. Riaz, R. Ellahi, N. S. Akbar, Effects of heat and mass transfer on peristaltic flow of a nanofluid between eccentric cylinders, Appl. Nanosci. 4 (2014) 393-404. https://doi.org/10.1007/s13204-013-0225-x.

[39] N. Ijaz, A. Zeeshan, M.M. Bhatti, R. Ellahi, Analytical study on liquid-solid particles interaction in the presence of heat and mass transfer through a wavy channel, J. Mol. Liq. 250 (2018) 80-87. https://doi.org/10.1016/j.molliq.2017.11.123.

[40] M.M. Bhatti, A. Zeeshan, R. Ellahi, Heat transfer analysis on peristaltically induced motion of particle-fluid suspension with variable viscosity: Clot blood model, Comput. Method Prog. Biomed. 137 (2016) 115-124. https://doi.org/10.1016/j.cmpb.2016.09.010.

[41] K. Ramesh, D. Tripathi, O. Anwar Bég, A. Kadir, Slip and Hall current effects on jeffrey fluid suspension flow in a peristaltic hydromagnetic blood micropump, Iran J. Sci. Technol. Trans. Mech. Eng. (2018) 1-18. https://doi.org/10.1007/s40997-018-0230-5.

[42] G. Xiong, J. Zhan, K. Zuo, J. Li, L. Rong, G. Xu, Numerical flow simulation in the post-endoscopic sinus surgery nasal cavity, Med. Biol. Eng. Comput. 46 (2008) 1161–1167. https://doi.org/10.1007/s11517-008-0384-1.

[43] A.E.M. El Misiery, Abd El Hakeem, Abd El Naby, Abd Hameed El Nagar, Effects of a fluid with variable viscosity and an endoscope on peristaltic motion, J. Phy. Soc. Japan 72 (2003) 89-93. https://doi.org/10.1016/j.amc.2003.09.008.

[44] D. Tripathi, Numerical study on peristaltic flow of generalized Burgers' fluids in uniform tubes in the presence of an endoscope, Int. J. Numer. Method Biomed. Eng. 27 (2011) 1812-1828. https://doi.org/10.1002/cnm.1442.

[45] T. Hayat, E. Momoniat, F.M. Mahomed, Endoscope effects on MHD peristaltic flow of a power-law fluid, Math. Prob. Eng. 2006 (2006) 84276. http://dx.doi.org/10.1155/MPE/2006/84276.

[46] Mekheimer KS, Abd Elmaboud Y, A. Abdellateef, Particulate suspension flow induced by sinusoidal peristaltic waves through eccentric cylinders: thread annular, Int. J. Biomath. 6 (2013) 1350026. https://doi.org/10.1142/S1793524513500265.

[47] M.M. Rashidi, M. Keimanesh, O. Anwar Bég, T.K. Hung, Magnetohydrodynamic biorheological transport phenomena in a porous medium: a simulation of magnetic blood flow control and filtration, Int. J. Numer. Meth. Bio. 27 (2011) 805-821. https://doi.org/10.1002/cnm.1420.

[48] D. Tripathi, O. Anwar Bég, Magnetohydrodynamic peristaltic flow of a couple stress fluid through coaxial channels containing a porous medium, J. Mech. Med. Biol. 12 (2012) 1250088. https://doi.org/10.1142/S0219519412500881.

[49] D. Tripathi, R. Jhorar, O. Anwar Bég and A. Kadir, Electro-magneto-hydrodynamic peristaltic pumping of couple stress biofluids through a complex wavy micro-channel, J. Mol. Liq. 236 (2017) 358-367. https://doi.org/10.1016/j.molliq.2017.04.037.

[50] M.M. Rashidi, Z. Yang, M.M. Bhatti, M.A. Abbas, Heat and Mass Transfer Analysis on MHD Blood Flow of Casson Fluid Model due to Peristaltic Wave, Therm. Sci. 22 (2018) 2439-2448. https://doi.org/10.2298/TSCI160102287R.

[51] Kh.S. Mekheimer, Peristaltic flow of a couple stress fluid in an annulus: application of an endoscope, Physica A Stat. Mech. Appl. 387 (2008) 2403-2415. https://doi.org/10.1016/j.physa.2007.12.017.

[52] O. Anwar Bég, L. Sim, J. Zueco and R. Bhargava, Numerical study of magnetohydrodynamic viscous plasma flow in rotating porous media with Hall currents and inclined magnetic field influence, Commun. Nonlinear Sci. 15 (2010) 345-359. https://doi.org/10.1016/j.cnsns.2009.04.008.

[53] O. Anwar Bég, S. Abdul Gaffar, V. Ramachandra Prasad, M.J. Uddin, Computational solutions for non-isothermal, nonlinear magnetoconvection in porous media with Hall/ionslip currents and Ohmic dissipation, Eng. Sci. Technol. Int J. 19 (2016) 377-394. https://doi.org/10.1016/j.jestch.2015.08.009.

[54] A. Riaz, S. Nadeem, R. Ellahi, N.S. Akbar, The influence of wall flexibility on unsteady peristaltic flow of Prandtl fluid in a three-dimensional rectangular duct, Appl. Math. Comput. 241 (2014) 389-400. https://doi.org/10.1016/j.amc.2014.04.046.

[55] J.H. He, Homotopy perturbation technique, Comput. Methods Appl. Mech. Eng. 178 (1999) 257-262. https://doi.org/10.1016/S0045-7825(99)00018-3.

[56] T. Alarabi, A.F. Elsayed, O Anwar Bég, Homotopy perturbation method for heat transfer in peristaltic flow of viscoelastic fluid in an eccentric cylinder with variable effects, Life Sci. J. 11 (2014) 197-206. https://doi.org/10.7537/marslsj110714.24.

[57] D. Tripathi, O. Anwar Bég, A numerical study of oscillating peristaltic flow of generalized Maxwell viscoelastic fluids through a porous medium, Transp. Porous Media. 95 (2012) 337-348. https://doi.org/10.1007/s11242-012-0046-5.

[58] M.M. Rashidi, A. Shooshtari, O. Anwar Bég, Homotopy perturbation study of nonlinear vibration of von Karman rectangular plates, Comput. Struct. 106/107 (2012) 46–55. https://doi.org/10.1016/j.compstruc.2012.04.004

[59] M.J. Uddin, O. Anwar Bég, A.I. Ismail, Radiative-convective nanofluid flow past a stretching/shrinking sheet with slip effects, J. Thermophys. Heat Tr. 29 (2015) 513-523. https://doi.org/10.2514/1.T4372.

[60] O. Anwar Bég, J. Zueco, M. Norouzi, M. Davoodi, A.A. Joneidi, A.F. Elsayed, Network and Nakamura tridiagonal computational simulation of electrically-conducting biopolymer micro-morphic transport phenomena, Comput. Biol. Med. 44 (2014) 44–56. https://doi.org/10.1016/j.compbiomed.2013.10.026.

[61] O. Anwar Bég, M. Ferdows, S. Islam, M. Nazrul Islam, Numerical simulation of Marangoni magnetohydrodynamic bio-nanofluid convection from a non-isothermal surface with magnetic induction effects: a bio-nanomaterial manufacturing transport model, J. Mech. Med. Biol. 14 (2014)1450039. https://doi.org/10.1142/S0219519414500390.

[62] N.S. Akbar, MHD Eyring–Prandtl fluid flow with convective boundary conditions in small intestines, Int. J. Biomath. 6 (2013) 1350034. https://doi.org/10.1142/S1793524513500344.

[63] A. Yıldırım, S.A. Sezer, Effects of partial slip on the peristaltic flow of a MHD Newtonian fluid in an asymmetric channel, Math. Comput. Model. 52 (2010) 618-625. https://doi.org/10.1016/j.mcm.2010.04.007.

[64] T. Hayat, S. Asghar, A. Tanveer, A. Alsaedi, Homogeneous–heterogeneous reactions in peristaltic flow of Prandtl fluid with thermal radiation, J. Mol. Liq. 240 (2017) 504-513. https://doi.org/10.1016/j.molliq.2017.05.058.

[65] O. Anwar Bég, J. Zueco, L.M. Lopez-Ochoa, Network numerical analysis of optically thick hydromagnetic slip flow from a porous spinning disk with radiation flux, variable thermophysical properties, and surface injection effects, Chem. Eng. Commun. 198 (2010) 360-384. https://doi.org/10.1080/00986445.2010.512543.

[66] K. Vafai**,** C.L. Tien, Boundary and inertia effects on flow and heat transfer in porous media, Int. J. Heat Mass Trans. 24 (1981) 195–203. https://doi.org/10.1016/0017-9310(81)90027-2.

[67] D. Tripathi, A. Sharma, O. Anwar Bég, Electrothermal transport of nanofluids via peristaltic pumping in a finite micro-channel: effects of Joule heating and Helmholtz-Smoluchowski velocity, Int. J. Heat Mass Transf. 111 (2017) 138–149. https://doi.org/10.1016/j.ijheatmasstransfer. 2017.03.089.

Nomenclature

$(\tilde{r}, \tilde{z})$	Cylindrical coordinate system
c	Velocity of the peristaltic wave
b_0	Radius of the outer tube inlet
K	Constant
$\tilde{a}$	Amplitude of the peristaltic wave
$b(\tilde{z})$	Radius of the outer tube
λ	Wavelength
a	Inner tube radius
$f\left(\tilde{z}, t\right)$	Arbitrary function
$\tilde{t}$	Time
v_0	Constant
$\tilde{U}, \tilde{V}$	Velocity components
B_0	Radius of a spherical particle suspended in the biofluid
C	Particle volume fraction
μ_s	Apparent (effective) viscosity
S	Drag coefficient
$\tilde{T}$	Temperature
$\mathbf{B}_0$	Applied radial magnetic field
J	Current density
μ_0	Fluid dynamic viscosity

σ	Electrical conductivity
$\mathbf{V}$	Velocity vector of the fluid
$\boldsymbol{e}$	Electron charge
n	Number of density electrons
δ	Maximum height of clot
z_d	Axial displacement of a clot
m	Hall parameter
$\hat{\theta}$	Embedding parameter
$Q(z,t)$	Volume flow rate
τ	Stress tensor
M	Hartmann number
φ	Amplitude ratio
α, β	Prandtl fluid parameters
$\tilde{P}$	Pressure
$\overline{\delta}$	Wave number
K	Permeability parameter

Subscripts

p	Particle phase
f	Fluid phase